

Radiation background studies for the LHC upgrade: Impact of machine magnets inside the ATLAS experiment.

I. Dawson, M. Shupe

Abstract

Various scenarios are being investigated for increasing the LHC luminosity, several of which require machine magnets positioned inside the ATLAS experiment. In this report we try to assess the implications of such machine upgrade scenarios on the ATLAS radiation backgrounds.

Contents

- 1. Introduction.**
- 2. Machine upgrade proposals.**
- 3. Impact of D0a on ATLAS.**
 - 3.1 Impact on inner detector fluences.
 - 3.2 Impact on forward calorimeter performance.
- 4. Impact of D0b on ATLAS.**
- 5. Impact of TAS inside JTT, with Q0a and Q0b inside JF**
- 6. Discussion and conclusion**
- 7. References**
- 8. GEANT/GCALOR result tables**

1. Introduction

Various scenarios are being investigated for increasing the LHC luminosity, several of which require machine magnets positioned inside the ATLAS experiment. In this report we try to assess the implications of such machine upgrade scenarios on the ATLAS radiation backgrounds. The simulation tools used in this analysis are the same ones used in the original Radiation Task Force (RTF) report¹. Minimum bias events are generated with PHOJET, followed by particle transport using FLUKA, or GEANT/GCALOR. Inner detector calculations have been done with FLUKA and GCALOR, whereas muon region calculations were obtained with GCALOR alone.

In order to assess the impact of an upgrade scenario, the radiation background predictions for each scenario are compared with baseline predictions and presented as ratios.

2. Machine upgrade proposals

In 2007, two upgrade schemes were proposed, both involving new beamline magnets inside the ATLAS experiment.

The first scheme, described in reference 2 (Sterbini *et al*) is based on two new compact dipoles; D0a, placed in front of the forward calorimeter, in the alcove currently occupied by a low-mass pump and neutron moderator; and D0b, placed behind the forward calorimeter in the volume currently occupied by the JD copper shield. D0a has low mass coils, and is ironless, but the heat load induced by ionizing radiation must be reduced by a tungsten ring placed upstream of this magnet. The D0b is a more conventional design with iron yoke. The primary focus of our simulation of this scheme was (1) increased radiation backgrounds in the inner detector due to secondaries produced in the tungsten ring, and (2) increased rates in the muon system, particularly the CSC region, due to the reduction of material inside the JD support tube. Simulations were done separately for D0a and D0b in order to study their impact on backgrounds individually.

The second scheme, described in reference 3 (Wildner), places two new slim quadrupoles, Q0a and Q0b, downstream of the forward calorimeter. In this scheme, the JD core is left unmodified, but a new TAS collimator is placed in the core of the JTT (inside the forward toroid) to reduce the heat load in Q0a and Q0b. Q0a is placed in the core of the JF shield, near its front end, while Q0b occupies the rear core of the JF shield and extends inside the monoblock, through the position of the current TAS. The concern in this design is that small apertures are being introduced along the beamline behind the forward calorimeter, creating new secondary sources that will increase background levels in the muon system.

3. Impact of D0a on ATLAS.

3.1 Impact on inner detector fluences.

For the FLUKA simulations, fluences in the inner tracker volume were obtained with and without the D0a magnets. Of particular interest are 1MeV neutron equivalent fluences, which are used to determine bulk damage to the silicon detectors. The geometry and material description of the D0a magnets were taken from reference 2. The mass of the D0a is dominated by a tungsten ring used to reduce heat load. Shown in Fig. 1 are the simulated 1MeV neutron equivalent fluences in the inner tracker volume, along with a picture of the D0a magnet and its proposed location in front of the FCal. The fluences assume an integrated luminosity of 3000fb^{-1} .

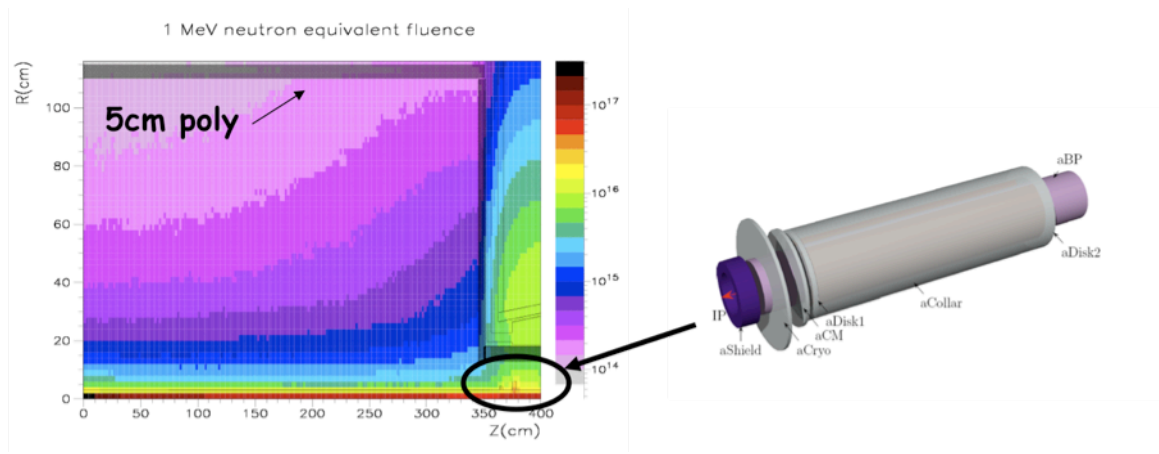


Fig.1: Quarter slice through FLUKA inner detector region, showing 1 MeV equivalent neutron fluences assuming an integrated luminosity of 3000fb^{-1} . Shown on the right is a picture of the proposed D0a magnet described in Ref. 2, which would be located in front of the ATLAS FCal.

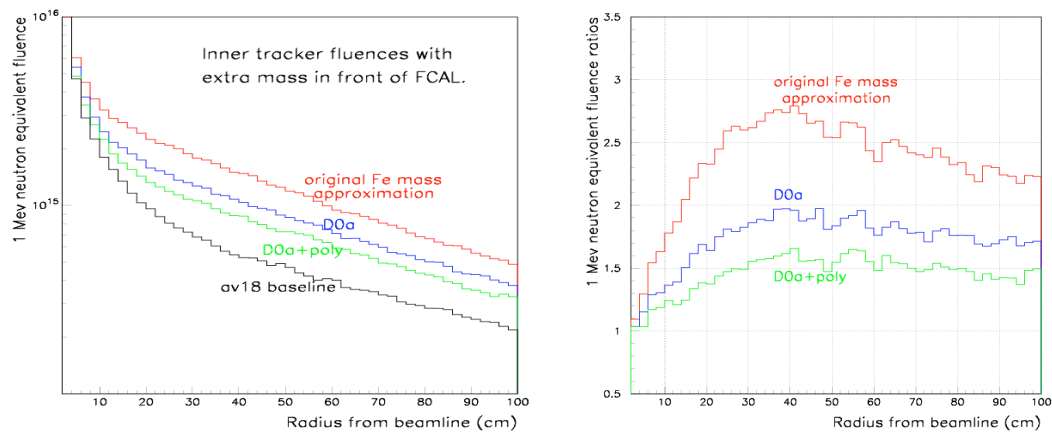


Fig. 2: The left plot shows 1 MeV equivalent neutron fluences in the inner tracker volume as a function of radius for $Z=300\text{cm}$. Three scenarios are compared with the av18 (no-magnet) baseline. The right plot gives the ratios.

In Fig. 2 the fluences are plotted as a function of radius, for $Z = 300\text{cm}$. It can be seen that beyond $\sim 30\text{cm}$ there is a significant increase in fluence when material is introduced in front of the FCAL. For radii smaller than $\sim 30\text{cm}$ the radiation backgrounds are dominated by particles from the pp interaction. The D0a magnet leads to an increase of approximately a factor 2, but this can be mitigated by adding additional polymoderator, as can be seen by the “D0a+poly” histogram. Also included in Fig. 2 are predictions for filling the most of the alcove region with iron, leading to increase in fluences up to a factor of ~ 3 . These increases in backgrounds are due to increased neutron albedo and are unavoidable when placing dense material near the beamline in the inner detector.

The FLUKA results are confirmed by GCALOR calculations. In the tables beginning “Impact of D0a on ...” in Section 8, the first table indicates up to factor 2 increase in 1 MeV neutron equivalent fluences, similar to the FLUKA study. Also included in these tables are particle fluence rates. It can be seen that photon and neutron fluences increase by up to factors of ~ 3 in the high-z forward regions.

The second ratio table in Section 8 shows that background rates in the muon system are affected very little by the D0a magnet, as expected.

The scoring regions used in the GCALOR simulations are shown in Figs. 3 and 4 of Section 8.

3.2 Impact on forward calorimeter performance.

The ATLAS forward calorimeter has been designed to give optimal position and energy resolution for forward/backward jets. This is achieved by maintaining the directionality of energy flow, maximizing containment of hadronic showers (through the use of tungsten in FCal modules 1 and 2), and making the transition to the other endcap calorimeters as seamless as possible. The tungsten ring in front of D0a in this scheme works counter to all of these strategies—causing showers to develop early and then fan out broadly by the time they impact the FCal and other endcap calorimeters. No detailed simulation has been done yet to look at the net effects on jet resolution, but judging from the large increases in inner detector backgrounds, we expect that the jet resolution would be noticeably degraded by the presence of the tungsten ring.

4. Impact of D0b on ATLAS

The D0b magnet would be downstream of the forward calorimeter, inside the JD support tube—replacing the copper alloy shielding that is there now. The radiation backgrounds increases in this design are due primarily to the net reduction of material in the JD region. In Section 8, the tables beginning “Impact of D0b on ...” show that background rates in the CSC/TGC region would increase by 20% to 40%, dependent on flux, and that increases elsewhere in the muon system have increases typically in the 10% to 20% range. (There are no increases in the inner detector due to D0b.) Whether these increases are serious or not depend on many other factors associated with upgrade design, and with simulation uncertainties (more below).

5. Impact of TAS inside JTT, with Q0a and Q0b inside JF

In reference 3, there are two designs for the TAS inside the JTT: the first is a solid cylinder and the second has an alcove region, or “catcher” in the first meter in an attempt to reduce albedo from the front surface. Also, for comparison with the ATLAS standard geometry, in all other simulations the beampipe has not been modified. But since there are also proposals to replace the forward region beampipes with beryllium pipes, this option was also simulated in this study. So there are four sets of tables for this scheme, in Section 8, “TAS in the JTT ...”, corresponding to the two TAS options and the two beampipe options.

The results are not difficult to summarize and understand:

- (1) There is no change in inner detector fluences due to these changes downstream.
- (2) Most of the muon region experiences increases by factors of 1.10 to 2.00, with the barrel region in general closer to the factor of 2.00
- (3) The catcher design *reduces* fluxes in the CSC/TGC region (near to it) by ~20%.

Inspection of the flux maps for these geometries shows that the second effect comes from the appearance of new ‘hot spots’ along the beamline due to the new TAS and quadrupoles. In the ATLAS standard design, the standard TAS is the hottest region in the experiment, and the forward calorimeter, the second-hottest. But in the current upgrade scheme, the new TAS and the two quadrupoles have small enough inner radii to intercept particles from the interaction point, so that three new hot spots show up within the JTT and JF region. The transverse flow of secondaries, and shower development, associated with these new sources penetrates the shielding throughout this region, creating a general increase in background rates in the muon system.

The third effect—the decrease of CSC/TGC rates by ~20% comes from the catcher design where the TAS hot spot is shifted one meter downstream, further from the CSC/TGC region. This design could have been employed in the standard shielding design, but it is undesirable because the resulting flux still shows up more generally in the muon system, as the current simulations illustrate.

6. Discussion and Conclusion.

We have simulated various machine upgrade scenarios and determined the impact on ATLAS radiation backgrounds. We conclude that:

- 1) Additional mass in front of the FCal will increase 1 MeV fluences in the inner detector regions—by up to a factor 3 in the worse case scenario. For the proposed D0a magnet a factor ~2 increase is observed, although with careful poly-moderator design this could be reduced to ~1.5. A D0a magnet does not impact fluences in the muon system, but would likely impact forward calorimeter performance.
- 2) Up to 40% increases in muon rates were observed in the CSC/TGC regions from the introduction of a D0b magnet. Increases elsewhere are typical in range 10% to 20%.
- 3) The impact of the “TAS and slim-line quadrupole” scenario” would be to increase muon rates by up to a factor 2.

There are two large issues that have not been addressed in this document, but that will be major factors affecting the choices of upgrade detector technologies.

The first is the issue of “safety factors”. These arise from uncertainties associated with event generators, particle transport codes, simulation geometry simplifications, detector element response, and detector and electronics damage. When concatenated, radiation background effects in the inner detector must generally be increased by a factor of 1.5, and in the muon region, by factors ranging from 2 to 5. There are several groups preparing to reduce these factors by measuring the backgrounds and their effects during the early operation of ATLAS. But until they are reduced, these factors are often comparable to, or considerably larger than, the effects that we have been discussing in this document!

The second issue is that the upgrade luminosity is expected to increase relative to the nominal luminosity by a factor of 7 to 10. But no shielding tactics have been found that reduce background rates by factors of more than 1.5 to 2, and these are most often for particular particle fluences, such as thermal neutrons. The essential problem is that in regions where the radiation shielding is critically thin, all available space has been occupied. Hundreds of simulations since the mid-1990’s have shown that there are no magical combinations of new materials that shield more effectively in these limited spaces—even if the funding were unlimited. Note that in all of the studies presented here, we have encountered increasing backgrounds in almost every case—which works in the wrong direction. The conclusion is that either (1) upgrade detectors must be redesigned to make more space in critically thin regions, or (2) the detectors must be able to withstand backgrounds that are *more* than a factor of 7 to 10 greater than those at the standard luminosity.

One can hope that the safety factors have turned out to be conservative. If the actual rates and damage effects correspond to safety factors of 1.0, then this in itself will offset many of the effects due to luminosity increase—at least in the muon regions. We will be revisiting all these issues as the actual backgrounds are measured.

7. References

- [1] M. Bosman et al, *Estimation of Radiation Background, Impact on Detectors, Activation and Shielding Optimization in ATLAS*, ATL-GEN-2005-001.
- [2] G. Sterbini et al, *Layout Version 1 for the Early separation scheme in ATLAS*, EDMS 848691.
- [3] E. Wildner, *Heat deposition and backscattering for one of the configurations of the IR for the LHC upgrade*, EDMS 860277

8. GEANT/GCALOR Results

ATLAS Background Radiation Calculations
 University of Arizona, M. Shupe
 Using GEANT3 with GCALOR interface (C. Zeitnitz)

Files and simulation statistics:
 11468 flux_STARTUP_12_25_11468.datf
 12228 flux_D0a_12_29_12228.datf
 9648 flux_D0b_12_29_9648.datf
 15568 fluxtem_TASJTT_12_31_15568.datf
 17776 fluxtem_TASJTT_CATCH_12_27_17776.datf
 5608 fluxtem_TASJTT_BEPIPE_12_25_5608.datf
 8140 fluxtem_TASJTT_CATCH_BEPIPE_12_8140.datf

ATLAS Geometry at Startup, 2008

Rates in Inner Detector:

GEOMETRY: Startup Base 11k	RATES (kHz/cm ²)					
	N<100k	N>100k	Photons	Pions	Had>20M	NEq/cm ² /Yr
Low Z Inner	1813.28	2195.30	29460.27	17009.72	25389.18	0.14E+15
Mid Z Inner	2087.68	2085.19	27692.12	12588.79	19270.08	0.10E+15
High Z Inner	2377.93	2708.23	37372.05	11890.57	18516.99	0.11E+15
Low Z Outer	1729.88	665.80	3818.32	349.45	550.16	0.11E+14
Mid Z Outer	1926.60	869.62	5701.83	368.12	617.33	0.13E+14
High Z Outer	2048.58	1149.31	7690.11	382.68	726.67	0.16E+14

Rates in Muon System:

GEOMETRY: Startup Base 11k	RATES (kHz/cm ²)					
	N<100k	N>100k	Photons	Had>20M	Counts	Triggers
SW CSC	59.130	29.800	37.207	6.885	0.619	0.1828
SW TGC	25.244	9.217	12.353	1.482	0.198	0.0507
LW MDT In	4.370	1.679	17.709	0.692	0.233	0.0437
LW MDT Out	4.238	1.267	6.987	0.560	0.097	0.0206
BW MDT In	2.611	0.797	2.161	0.086	0.032	0.0073
B RPC HiZMid	4.525	1.211	1.970	0.246	0.031	0.0077
B RPC HiZOut	4.118	0.956	1.928	0.229	0.029	0.0058

Early Separation Scheme (Ref 2), with dipoles D0a and D0b

Impact of D0a on inner detector

FLUX RATIO:	UPG D0a 12k / Startup Base 11k					
	N<100k	N>100k	Photons	Pions	Had>20M	NEq/cm2/Yr
Low Z Inner	1.46	1.15	1.10	1.01	1.01	1.02
Mid Z Inner	1.73	1.52	1.34	1.01	1.01	1.11
High Z Inner	2.26	2.98	2.16	1.01	1.03	1.53
Low Z Outer	1.41	1.33	1.58	1.03	1.04	1.20
Mid Z Outer	1.65	1.80	2.34	1.04	1.10	1.55
High Z Outer	1.74	2.17	2.56	1.05	1.19	1.88

Impact of D0a on muon system

FLUX RATIO:	UPG D0a 12k / Startup Base 11k					
	N<100k	N>100k	Photons	Had>20M	Counts	Triggers
SW CSC	1.02	1.05	1.03	1.07	1.01	0.96
SW TGC	1.02	1.05	1.02	1.04	1.02	1.00
LW MDT In	1.02	0.97	1.01	0.95	1.00	0.96
LW MDT Out	1.02	1.00	1.03	1.00	1.05	1.13
BW MDT In	1.03	1.00	1.01	0.96	0.98	0.88
B RPC HiZMid	1.03	1.04	1.04	1.03	1.02	0.94
B RPC HiZOut	1.01	1.01	1.02	1.02	1.00	0.94

Impact of D0b on inner detector

FLUX RATIO:	UPG D0b 10k / Startup Base 11k					
	N<100k	N>100k	Photons	Pions	Had>20M	NEq/cm2/Yr
Low Z Inner	1.00	1.00	0.99	1.00	0.99	0.96
Mid Z Inner	0.99	1.00	1.00	0.99	1.00	0.96
High Z Inner	0.99	1.00	1.00	0.99	1.00	0.96
Low Z Outer	0.99	0.99	0.99	0.99	0.99	0.99
Mid Z Outer	0.99	0.99	1.00	0.99	0.99	0.99
High Z Outer	1.00	0.99	0.98	0.99	0.99	0.99

Impact of D0b on muon system

FLUX RATIO:	UPG D0b 10k / Startup Base 11k					
	N<100k	N>100k	Photons	Had>20M	Counts	Triggers
SW CSC	1.31	1.34	1.25	1.25	1.23	1.16
SW TGC	1.22	1.38	1.25	1.32	1.25	1.25
LW MDT In	1.07	1.00	1.01	1.03	1.01	1.01
LW MDT Out	1.15	1.08	1.05	1.04	1.07	1.14
BW MDT In	1.04	1.02	1.06	1.03	1.05	1.03
B RPC HiZMid	1.21	1.28	1.21	1.23	1.21	1.20
B RPC HiZOut	1.19	1.17	1.16	1.15	1.13	1.01

TAS in the JTT with quadrupoles Q0a and Q0b (Reference 3)

Impact of standard TASJTT with standard beampipe on inner detector:

FLUX RATIO:	TASinJTT 15K / Startup Base 11k					
	N<100k	N>100k	Photons	Pions	Had>20M	NEq/cm2/Yr
Low Z Inner	1.00	1.00	1.06	1.02	1.06	0.97
Mid Z Inner	0.99	1.00	1.03	1.00	1.00	1.02
High Z Inner	1.00	1.00	1.13	1.00	1.00	1.02
Low Z Outer	1.00	0.99	1.00	0.99	0.99	0.99
Mid Z Outer	0.99	1.00	1.10	1.00	1.00	1.00
High Z Outer	1.00	1.00	1.15	0.99	0.99	0.99

Impact of standard TASJTT with standard beampipe on muon system:

FLUX RATIO:	TASinJTT 15K / Startup Base 11k					
	N<100k	N>100k	Photons	Had>20M	Counts	Triggers
SW CSC	1.13	1.12	0.97	1.10	1.00	1.02
SW TGC	1.21	1.31	1.34	1.33	1.31	1.28
LW MDT In	1.20	0.80	0.30	0.77	0.38	0.67
LW MDT Out	1.88	1.49	0.73	1.29	0.86	1.19
BW MDT In	2.23	1.95	1.37	1.45	1.39	1.27
B RPC HiZMid	1.90	1.90	2.04	1.96	1.96	1.78
B RPC HiZOut	2.04	2.26	2.18	2.47	2.14	2.03

Impact of TASJTT with Catcher and standard beampipe on inner detector:

FLUX RATIO:	TASCatch 17K / Startup Base 11k					
	N<100k	N>100k	Photons	Pions	Had>20M	NEq/cm2/Yr
Low Z Inner	1.00	1.00	1.06	1.01	1.05	0.99
Mid Z Inner	0.99	1.00	1.03	1.00	1.00	1.03
High Z Inner	1.00	1.00	1.12	1.00	1.00	1.03
Low Z Outer	1.00	0.99	1.00	0.99	0.99	1.00
Mid Z Outer	1.00	1.00	1.09	1.00	1.00	1.00
High Z Outer	1.00	1.00	1.13	0.99	0.99	1.00

Impact of TASJTT with Catcher and standard beampipe on muon system:

FLUX RATIO:	TASCatch 17K / Startup Base 11k					
	N<100k	N>100k	Photons	Had>20M	Counts	Triggers
SW CSC	1.05	1.06	0.87	1.03	0.91	0.98
SW TGC	1.15	1.18	1.19	1.14	1.17	1.12
LW MDT In	1.31	1.15	0.37	1.27	0.46	0.77
LW MDT Out	1.98	1.83	0.84	1.74	1.00	1.46
BW MDT In	2.24	1.93	1.41	1.43	1.46	1.44
B RPC HiZMid	1.93	1.89	2.06	1.94	2.00	1.88
B RPC HiZOut	2.08	2.30	2.23	2.43	2.17	1.98

Impact of standard TASJTT with beryllium beampipe on inner detector:

FLUX RATIO:	TASJTTBe 6K / Startup Base 11k					
	N<100k	N>100k	Photons	Pions	Had>20M	NEq/cm2/Yr
Low Z Inner	0.98	0.99	0.97	0.99	0.98	0.95
Mid Z Inner	0.97	0.98	0.95	1.00	0.99	0.95
High Z Inner	0.96	0.96	0.89	1.00	0.99	0.95
Low Z Outer	0.98	0.97	0.92	0.99	0.98	0.97
Mid Z Outer	0.97	0.97	0.91	0.99	0.98	0.97
High Z Outer	0.97	0.96	0.90	0.98	0.97	0.96

Impact of standard TASJTT with beryllium beampipe on muon system:

FLUX RATIO:	TASJTTBe 6K / Startup Base 11k					
	N<100k	N>100k	Photons	Had>20M	Counts	Triggers
SW CSC	0.79	0.78	0.69	0.76	0.73	0.80
SW TGC	0.92	0.99	1.05	1.00	1.03	1.00
LW MDT In	1.19	0.89	0.31	0.84	0.38	0.61
LW MDT Out	1.83	1.53	0.74	1.37	0.86	1.18
BW MDT In	2.08	1.76	1.32	1.20	1.31	1.13
B RPC HiZMid	1.76	1.73	1.93	1.79	1.86	1.72
B RPC HiZOut	1.96	2.23	2.11	2.45	2.07	1.96

Impact of TASJTT with Catcher and beryllium beampipe on inner detector:

FLUX RATIO:	TASCatBe 8K / Startup Base 11k					
	N<100k	N>100k	Photons	Pions	Had>20M	NEq/cm2/Yr
Low Z Inner	1.00	1.00	1.04	1.01	1.06	1.02
Mid Z Inner	0.98	0.99	0.96	1.01	1.00	1.05
High Z Inner	0.98	0.97	0.93	1.00	1.00	1.04
Low Z Outer	0.99	0.99	0.94	1.00	1.00	0.99
Mid Z Outer	0.99	0.98	0.95	1.00	1.00	0.99
High Z Outer	0.98	0.98	1.07	1.00	0.99	0.98

Impact of TASJTT with Catcher and beryllium beampipe on muon system:

FLUX RATIO:	TASCatBe 8K / Startup Base 11k					
	N<100k	N>100k	Photons	Had>20M	Counts	Triggers
SW CSC	0.71	0.72	0.59	0.72	0.66	0.78
SW TGC	0.86	0.84	0.91	0.77	0.89	0.88
LW MDT In	1.31	1.33	0.41	1.53	0.50	0.84
LW MDT Out	1.96	1.95	0.87	1.95	1.04	1.54
BW MDT In	2.12	1.80	1.40	1.28	1.42	1.34
B RPC HiZMid	1.78	1.76	1.95	1.79	1.87	1.69
B RPC HiZOut	2.00	2.28	2.19	2.43	2.13	1.95

GCALOR scoring regions

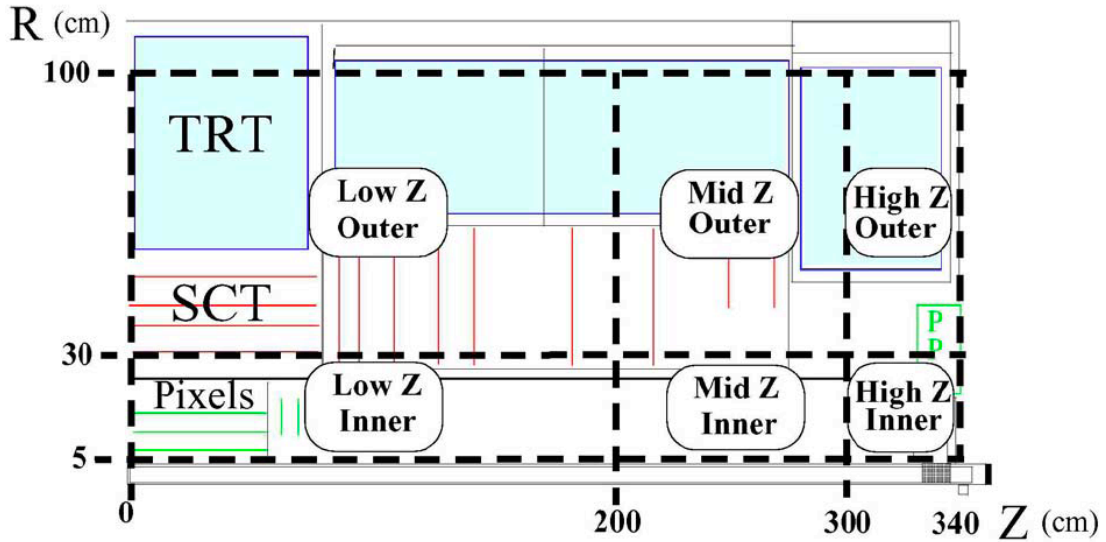


Fig.3: Quarter slice through ATLAS inner detector geometry, indicating GCALOR scoring regions

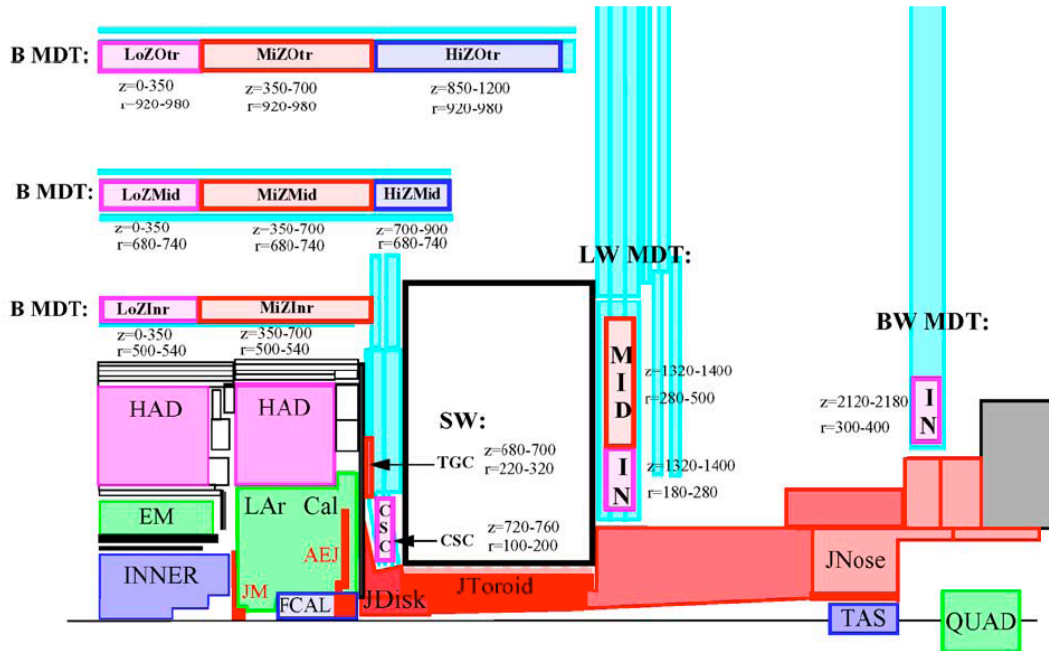


Fig.4: Quarter slice through ATLAS geometry, indicating GCALOR scoring regions in muon system.